Highlights

Focusing gain analysis in time-reversal precoding MISO OFDM communication systems

Trung-Hien Nguyen, Jean-François Determe, Shaghayegh Monfared, Jérôme Louveaux, Philippe De Doncker, François Horlin

- We quantify the focusing gain (FG) of frequency-domain time-reversal (FD/TR) precoding in a multiple-input single-output (MISO) orthogonal frequency-division multiplexing (OFDM) system with different numbers of antennas and rate back-off factors (BOFs).
- We derive approximated mean-square-error (MSE) expressions at either the intended or unintended positions, and the subsequent FG formula, for the FD/TR precoding MISO OFDM systems. Similarly to time-domain (TD) TR precoding, the MSE of the received symbols at the intended position is shown to be lower than that at the unintended position, confirming again the focusing gain of the FD/TR precoding.
- In order to obtain the MSE approximation at the unintended position, we derive the probability density function (PDF) of the modulus of the sum of products of zero-mean complex Gaussian random variables (RVs) with arbitrary variances. Furthermore, based on the shapes of PDFs of the equivalent channel RVs at the intended and unintended positions, we intuitively show that the diversity and focusing gains at the intended position is bigger than that at the unintended position.
- We analyze the asymptotic behavior of the MSE expressions to gain insights in the tendencies evolution of the MSE at either intended or unintended positions.
- We carry out numerical simulations with multi-path Rayleigh fading channels to validate our analyses.

Focusing gain analysis in time-reversal precoding MISO OFDM communication systems*

Trung-Hien Nguyen[a,*], Jean-François Determe[a], Shaghayegh Monfared[a], Jérôme Louveaux[b], Philippe De Doncker[a] and François Horlin[a]

[a]OPERA department, Université libre de Bruxelles (ULB), 1050 Brussels, Belgium
[b]ICTEAM institute, Université catholique de Louvain (UCL), 1348 Louvain-la-Neuve, Belgium

ARTICLE INFO

Keywords:
time-reversal
rate back-off factor
OFDM

ABSTRACT

Emerging communication systems can benefit from time-reversal (TR) technology thanks to its good spatio-temporal signal focusing effect. The recent advances in low-cost wideband devices fabrication further leverage the use of TR wideband communication systems. The TR is generally carried out in the time domain and the focusing effect of TR comes from the use of a high rate back-off factor (BOF), which is the signal up-sampling (or down-sampling) rate. In spite of the widely-used orthogonal frequency-division multiplexing (OFDM) modulation, a few works have investigated the frequency-domain TR precoding in combination with OFDM communication systems. Furthermore, most of existing FD precoding works rely on multiple-antenna technology to create the focusing effect. In this paper, we investigate the focusing gain provided by TR precoding in multiple-input single-output (MISO) OFDM systems. In particular, we compare the communication performance of such system at the intended position and that at the unintended position. Based on the analysis, we demonstrate that increasing the BOF and/or the number of transmit antennas significantly improves the focusing effect at the intended position. In contrast, the unintended positions receive less useful power. We derive approximated mean-square-error (MSE) expressions of equalized received signals at both intended and unintended positions. The subsequent focusing gain is presented as a function of the BOF and the number of antennas, enabling us to gain insights in the contributions of each parameter to the system performance. Numerical simulations with multi-path Rayleigh fading channels are carried out to validate the MSE expressions.

1. Introduction

Time-reversal (TR) is a simple and efficient matched-filter technology for emerging communication systems [1]. It has been shown that with a sufficiently high rate back-off factor (BOF), the TR can constructively combine the energy from different multipath components, in order to create a spatio-temporal focusing effect [2]. TR precoding can be implemented in either time-domain (TD) or frequency-domain (FD). In the literature, TD/TR precoding has been well studied [2]. The focusing effect of the TD/TR precoding comes from the use of a high BOF, which is defined as the signal up-sampling rate at the transmitter before the precoding process (or the respective signal down-sampling rate at the receiver before equalization). Because of the spatio-temporal focusing effect of TD/TR precoding systems, a one-tap equalizer is generally sufficient in such systems enabling a complexity reduction at the receiver.

Orthogonal frequency-division multiplexing (OFDM) is nowadays a widely-used modulation in new generation wireless systems, as it facilitates the equalization of frequency-selective channels. Moreover, the multiple-input single-output (MISO) OFDM system in combination with the FD/TR precoding has been shown to be a simple and efficient technology in a distributed-antenna communication system [3, 4]. However, previous works have implicitly dealt with BOFs equal to one; thereby, the system does not fully benefit from the focusing effect of TR. Recently, the FD/TR precoding has been investigated with BOFs different from one [5]. However, only the system performance at the intended communication position was considered; hence, compared to the other unintended positions, the focusing gain stemming from TR at the intended position was not studied.

In this paper, we investigate the focusing gain (FG) of the FD/TR precoding in MISO OFDM systems when varying the number of antennas and/or BOFs. The focusing gain is defined by the signal-to-noise ratio (SNR) gain necessary

*This document is the research results funded by the Copine-IoT Innoviris project, the Icity.Brussels project and the FEDER/EFRO grant.
*Corresponding author: trung-hien.nguyen@ulb.ac.be
ORCID(s): 0000-0001-9828-5769 (T. Nguyen)

to keep the mean-square-error (MSE) of the received signals unchanged when switching from the intended position to the unintended position. Our main contributions can be summarized as follows:

- We assess for the first time the FG of the FD/TR precoding MISO OFDM system with different number of antennas and BOFs.
- We derive approximated MSE expressions at the intended and unintended positions, and the subsequent FG, for the FD/TR precoding MISO OFDM systems. Similarly to the TD/TR precoding, the MSE of the received symbols at the intended position is shown to be much lower than that at the unintended position, confirming the focusing gain of the FD/TR precoding.
- In order to obtain the MSE approximation at the unintended position, we derive the probability density function (PDF) of the modulus of the sum of products of zero-mean complex Gaussian random variables (RVs) with arbitrary variances. Furthermore, based on the shapes of PDFs of the equivalent channel RVs at the intended and unintended positions, we intuitively show that the diversity and focusing gains at the intended position is bigger than that at the unintended position.
- We analyze the asymptotic behaviors of the MSE expressions to understand in a simple manner the impacts of different used numbers of antennas and BOFs on the MSE when switching from the intended position to the unintended position. Finally, numerical simulations are carried out to validate our analysis.

The remainder of this paper is organized as follows: we present a brief overview of TR in Section II; the TR-based system model and the proper way to perform TR precoding in the FD are introduced in Section III; we carry out theoretical performance analyses in Section IV; the asymptotic analysis is conducted in Section V; we present our analytical and numerical results in Section VI; finally, the paper is concluded in Section VII.

Notation: Lower-case and upper-case bold letters denote column vectors and matrices, respectively; $\mathbf{I}_N$ is the $N\times N$ identity matrix; $\mathbf{F}_Q$ is the $Q \times Q$ Fourier matrix; $\mathbf{\Lambda}_{\mathbf{x}}$ is the diagonal matrix whose diagonal entries are the elements of the vector $\mathbf{x}$; $|\cdot|$, $||\cdot||$, $(\cdot)^*$, $(\cdot)^T$, $(\cdot)^H$ are the absolute value, Euclidean norm, complex conjugate, transpose and Hermitian transpose operators, respectively; $\mathrm{tr}\{\cdot\}$ and $\mathbb{E}[\cdot]$ are the trace and expectation operators, respectively; $x!$ is the factorial of a positive integer x.

2. Time-reversal history

The TR technique was invented to focus the wave energy into one position over the space [6]. Actually, the TR has been first proposed in 1950's in [7], where it was applied to alleviate the delay distortion in a picture transmission system. TR was then investigated in the digital communication in the 1960's, and it has been shown to be the optimal solution of a minimum-transmission-loss constrained optimization problem in the digital communication systems [8].

TR had been leveraged to improve the performances of the ultrasonic and acoustics systems [9], [6]. Since the nineties, TR has been applied in a lot of applications based on its spatio-temporal focusing effect. For example, the TR imaging technique has been proposed to identify multiple targets within a specific area in combination with the multiple signal classification (MUSIC) algorithm [10]. Target detection using TR-based antenna arrays has been investigated in multipath scattering environments [11]. Recently, TR has been claimed to be a promising candidate for 5G communication systems, where massive multipaths (one of the major challenges in modern wireless communications) are exploited to enhance the communication link instead of trying to remove them [12]. TR is also shown to be an interesting technology to provide physical layer security [13], centimeter-accuracy indoor localization [14, 15, 16], event detection through a wall [17], and monitoring of vital signs [18]. It is worth noticing that almost all TR-based applications referred here are in the TD. The FD/TR applications, however, did not consider the equivalent TR version as originally invented, i.e., that for which BOF is larger than one.

Due to the fact that OFDM modulation is used widely nowadays – especially in 5G networks, which leverage the use of FD precoding techniques for complexity reduction – the aforementioned TD/TR precoding cannot be easily integrated into modern communication systems. In what follows, we discuss in detail the FD/TR precoding. It is worth noticing that, in the literature, the intended position in some contexts, i.e., secure communications [13], is named as target or legitimate position, while the unintended positions are referred to as the eavesdropper or illegal or non-legitimate positions. In order to make terminologies coherent, we use the "intended position" and "unintended position" terms in this paper.

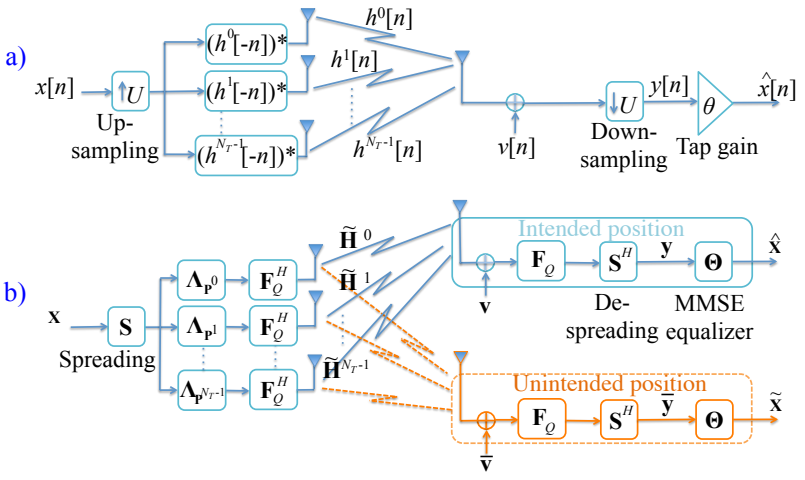

Figure 1: Schematics of (a) the TD/TR precoding communication system [2] and (b) the corresponding FD/TR precoding OFDM system when communicating with either intended or unintended positions.

3. System model

Figure 1(a) presents a typical TD/TR precoding MISO system [2], where the TD symbol sequence $x[n]$ is firstly up-sampled by a BOF U before being repeated on N_T transmit antenna branches. The signals are then pre-filtered by the TR precoder, $(h^k[-n])^*$, of the associated k-th channel impulse response (CIR), $h^k[n]$. Afterthat, the signals are sent over antennas. At the receiver side, the signal corrupted by additive white Gaussian noise (AWGN) $v[n]$ is down-sampled by U. The received signal can be equalized by a tap gain θ, which can be designed based on the minimum mean square error (MMSE) criterion. It is well-known in the literature [2] that the spatio-temporal focusing gain is improved in accordance with using more antennas and/or increasing the BOF. Hence, a better bit-error-ratio (BER)/MSE performance can be achieved at the cost of the signal rate reduction. Note that, the TD/TR precoding system requires a wideband analog-to-digital converter (ADC) at the receiver. However, we can sample the received signal directly at a low rate, which is equivalent to the rate after the down-sampling by the BOF, thereby simplifying the signal processing.

As aforementioned, the performance of FD/TR precoding OFDM system in previous works was only assessed for a varying number of antennas [3, 4] with the BOF implicitly equal to one. Recently, a proper way of TR precoding in the frequency domain has been presented in [5]. We recall here the method to properly assign the data symbols onto OFDM subcarriers in FD/TR precoding system (Fig. 1(b)). For simplicity, we consider that a single Q-subcarrier OFDM symbol is sent over the TR precoding MISO OFDM system. We transmit a data vector $\mathbf{x}$ composed of N symbols X_n (for $n = 0, 1, ..., N-1$ with $N = Q/U$) over the FD/TR precoding system, i.e., $\mathbf{x} = [X_0 \ ... \ X_{N-1}]^T$. The symbols $\{X_n\}$ are assumed to be independent zero-mean complex RVs with variance $\mathbb{E}[|X_n|^2] = \sigma_X^2$. Without loss of generality, a normalized constellation, $\sigma_X^2 = 1$, is considered.

The data symbols $\mathbf{x}$ are then spread by the matrix $\mathbf{S}$ of size $Q \times N$. The $Q \times N$ matrix $\mathbf{S}$ is the concatenation of U independent $N \times N$ diagonal matrices, whose diagonal values are identically and independently distributed and taken from the set $\{\pm 1\}$. The spreading matrix is normalized by $\sqrt{U}$ in order to get $\mathbf{S}^H\mathbf{S} = \mathbf{I}_N$. Thanks to the spreading matrix, the BOF discussed in the original TD/TR precoding is properly introduced. The idea behind this spreading comes from the fact that up-sampling a signal in the TD is equivalent to the repetition and shifting of its spectrum in the FD. Furthermore, a randomized spreading code is used to avoid assigning the same data symbol on different OFDM subcarriers, which causes a high peak-to-average-power ratio (PAPR) [19].

After spreading, the signal is repeated on N_T branches corresponding to transmit antennas and pre-coded by a matrix $\mathbf{\Lambda}_{\mathbf{p}^k}$ on each branch k. Defining $\mathbf{h}^k \triangleq [H_0^k \ H_1^k \ ... \ H_{Q-1}^k]^T$ as the channel frequency response (CFR) associated with the $k-$th antenna and assuming its associated channel power is normalized to unity, then $\mathbf{\Lambda}_{\mathbf{p}^k}$ is the diagonal matrix, whose diagonal elements are $(H_q^k)^*$ (for $q = 0, 1, ..., Q-1$). The FD/TR precoded signals are transformed to TD signals by using an inverse fast Fourier transform (IFFT) operator. The signal is then made cyclic by adding/removing

a cyclic prefix (CP) and propagated over the channel, which is mathematically equivalent to the multiplication with the $Q \times Q$ circulant matrix $\widetilde{\mathbf{H}}^k$ of the $k-$th CIR. The matrix $\widetilde{\mathbf{H}}^k$ can be factorized as $\widetilde{\mathbf{H}}^k = \mathbf{F}_Q^H \cdot \mathbf{\Lambda}_{\mathbf{h}^k} \cdot \mathbf{F}_Q$, where $\mathbf{\Lambda}_{\mathbf{h}^k}$ is the diagonal matrix, whose diagonal elements are the elements of vector $\mathbf{h}^k$. It is worth noticing that $\mathbf{\Lambda}_{\mathbf{h}^k}$ is associated to an arbitrary position, which may or may not be the intended position, i.e., that for which the precoding matrix $\mathbf{\Lambda}_{\mathbf{p}^k}$ is computed. At the receiver, the reversed operations are carried out. Note that, a wide-bandwidth ADC is required and a high sampling rate is needed as in conventional OFDM systems. However, the de-spreading operation reduces the sample rate to the symbol rate, thereby enabling the receiver to work at a *low-rate processing*. Assuming the time and frequency synchronization is perfect, the received signal after de-spreading at the intended position is given by

$$\mathbf{y} = \mathbf{S}^H \cdot \mathbf{F}_Q \cdot \left(\sum_{k=0}^{N_T-1} \widetilde{\mathbf{H}}^k \cdot \mathbf{F}_Q^H \cdot \mathbf{\Lambda}_{\mathbf{p}^k} \right) \cdot \mathbf{S} \cdot \mathbf{x} + \mathbf{v}', \tag{1}$$

where $\mathbf{v}' = \mathbf{S}^H \mathbf{F}_Q \mathbf{v} \triangleq [V'_0 \ ... \ V'_{N-1}]^T$ is the equivalent FD circularly symmetric complex AWGN of the TD AWGN $\mathbf{v}$. We assume that the signal X_n and noise V'_n are independent of each other. We define the noise auto-correlation matrix as $\mathbf{R}_{\mathbf{vv}} \triangleq \mathbb{E}\left[\mathbf{v} \cdot \mathbf{v}^H\right] = \sigma_V^2 \mathbf{I}_Q$, where σ_V^2 is the variance of $\mathbf{v}$. Based on the definition of the spreading matrix, we can deduce $\mathbf{R}_{\mathbf{v}'\mathbf{v}'} = \sigma_V^2 \mathbf{I}_N$. After some manipulations, (1) can be rewritten as $\mathbf{y} = \mathbf{G} \cdot \mathbf{x} + \mathbf{v}'$, where $\mathbf{G} = \mathbf{S}^H \cdot \left(\sum_{k=0}^{N_T-1} \mathbf{\Lambda}_{\mathbf{h}^k} \cdot \mathbf{\Lambda}_{\mathbf{p}^k} \right) \cdot \mathbf{S}$.

Similarly to the TD/TR system, we use a one-tap MMSE equalizer after de-spreading in order to recover the transmitted signal. By multiplying $\mathbf{y}$ with the MMSE equalizer matrix, given by $\mathbf{\Theta} = \left(\mathbf{G}^H \cdot \mathbf{G} + \gamma^{-1} \mathbf{I}_N\right)^{-1} \cdot \mathbf{G}^H$ (in which $\gamma \triangleq \sigma_X^2 / \sigma_V^2$ is the definition of the SNR), we obtain the estimate $\widehat{\mathbf{x}}$ of the input signal vector. It is worth noticing that if the TR precoding is matched to the channel, $\mathbf{\Theta}$ is a real-valued diagonal matrix, leading to a *low-complexity equalizer* at the receiver. At the unintended position, the same mathematical model can be built similarly. In order to make a fair performance comparison between intended and unintended positions, we assume that the same AWGN is inserted at both positions. Furthermore, the MMSE equalizer is also applied at the unintended position with the knowledge of the equivalent channel. Note that, the TR precoding is not matched to the channels at the unintended position, consequently $\mathbf{\Theta}$ is now a complex-valued diagonal matrix, thereby requiring more receiver complexity.

4. Performance Assessment

By defining $\mathbf{e} \triangleq \mathbf{x} - \widehat{\mathbf{x}}$ and $\mathbf{R}_{\mathbf{ee}} \triangleq \mathbb{E}\left[\mathbf{e} \cdot \mathbf{e}^H\right]$ and after some manipulations, the MSE of the equalized received symbol can be derived as follows[1]

$$MSE = \mathrm{tr}\left\{\mathbf{R}_{\mathbf{ee}}\right\} = \sigma_V^2 \mathrm{tr}\left\{\mathbb{E}\left[\left(\mathbf{G}^H \cdot \mathbf{G} + \gamma^{-1} \mathbf{I}_N\right)^{-1}\right]\right\}. \tag{2}$$

In order to assess the focusing gain of TR, we compare the normalized MSEs (NMSEs) (defined as $NMSE \triangleq MSE / \left(N \sigma_X^2\right)$) of the received signal at both the intended and unintended communication positions. Due to the fact that $\mathbf{G}$ is a diagonal matrix, the NMSE is given by

$$NMSE = \frac{1}{N} \sum_{n=0}^{N-1} \mathbb{E}\left[\frac{\gamma^{-1}}{\frac{1}{U^2}\left|K_n\right|^2 + \gamma^{-1}} \right], \tag{3}$$

where K_n is a random variable (RV) depending on the channel realization. More particularly, at the intended position, $K_n = \sum_{k=0}^{N_T-1} \sum_{u=0}^{U-1} \left| H_{n+uN}^k \right|^2$ and at the unintended position, $K_n = \sum_{k=0}^{N_T-1} \sum_{u=0}^{U-1} \overline{H}_{n+uN}^k \cdot \left(H_{n+uN}^k \right)^*$, in which $\overline{H}_n^k$ is the n-th component of the unintended position CFR associated with the k-th transmit antenna. We assume that the channels at the intended and unintended postions are spatially independent.

We further assume that the CIRs between each transmit antenna and the receive antenna comprise no more than L taps and are independent (i.e., constructed by uncorrelated scatterers). The variance of the l-th CIR tap is $\sigma_{h_l}^2 =$

[1] In what follows, the expectations are implicitly taken over the transmitted signal, noise and channel RVs.

$\mathbb{E}\left[\left|h_l\right|^2\right]$. Note that, a Rayleigh fading channel is considered in our case. Thanks to the design of spreading matrix $\mathbf{S}$ as described in Section 3, the RV K_n in (3) is constructed by the sum of weakly correlated complex RVs. When the BOF value is small or moderate, RVs H^k_{n+uN} and $H^k_{n+(u+1)N}$ (for $\forall n \in [0, N-1]$, $\forall k \in [0, N_T-1]$ and $\forall u \in [0, U-2]$) can be considered to be independent from one to another and identically distributed so that the NMSE in (3) can be approximated by

$$NMSE \approx \mathbb{E}\left[\frac{\gamma^{-1}}{\frac{1}{U^2}\left|K_n\right|^2 + \gamma^{-1}}\right]. \tag{4}$$

- At the intended position:

Although the NMSE has been derived in [5], we reproduce it here to facilitate the evaluation of the FG. Furthermore, more series expansion terms, i.e., second and third orders of the Taylor series expansion (detailed in the Appendix A), are used here to improve the approximation. The RV K_n has the PDF $f_Z(z) = z^{M-1}\mathrm{e}^{-z}/(M-1)!$ [20], where $M = UN_T$. Applying this PDF to (4), we obtain a closed-form NMSE expression

$$NMSE \approx \frac{\gamma^{-1}}{(M-1)!}\int_0^\infty \frac{z^{M-1}}{z^2/U^2 + \gamma^{-1}}\mathrm{e}^{-z}dz. \tag{5}$$

Although (5) can be numerically computed, it is still difficult to analyze the asymptotic behaviors. We therefore approximate (5) as in the Appendix A to yield a tractable NMSE approximation at the intended position, $f_{int}\left(\gamma, U, N_T\right)$, as follows

$$\begin{aligned} f_{int}\left(\gamma, U, N_T\right) \approx \frac{1}{\left(UN_T-1\right)!}\Bigg(&\Gamma_{low}\left(UN_T, U\gamma^{-1/2}\right) - \frac{1}{U^2\gamma^{-1}}\Gamma_{low}\left(UN_T+2, U\gamma^{-1/2}\right) \\ &+ \frac{1}{U^4\gamma^{-2}}\Gamma_{low}\left(UN_T+4, U\gamma^{-1/2}\right) + U^2\gamma^{-1}\Gamma_{up}\left(UN_T-2, U\gamma^{-1/2}\right) \\ &- U^4\gamma^{-2}\Gamma_{up}\left(UN_T-4, U\gamma^{-1/2}\right)\Bigg). \end{aligned} \tag{6}$$

in which Γ_{low} and Γ_{up} are the lower and upper incomplete Gamma functions, respectively, and defined by

$$\Gamma_{low}(a,t) = \int_0^t x^{a-1}\mathrm{e}^{-x}dx, \tag{7}$$

and

$$\Gamma_{up}(a,t) = \int_t^\infty x^{a-1}\mathrm{e}^{-x}dx, \tag{8}$$

such that $\Gamma_{low}(a,t) + \Gamma_{up}(a,t) = \Gamma(a)$ is the Gamma function.

- At the unintended position:

In order to derive a closed-form NMSE approximation, we have to know the PDF of the RV $\left|K_n\right|$. This PDF is derived in the following theorem.

Theorem 1. *Let a RV $Z_m = Y_{1,m} \cdot Y_{2,m}$, where $Y_{1,m}$ and $Y_{2,m}$ are statistically independent and identically distributed (i.i.d) complex Gaussian RVs of zero-mean and variance $\sigma^2_{Y_1}$ and $\sigma^2_{Y_2}$, respectively, i.e., $Y_{1,m} \sim \mathcal{CN}(0, \sigma^2_{Y_1})$, $Y_{2,m} \sim \mathcal{CN}(0, \sigma^2_{Y_2})$. Considering $Z = \sum_{m=0}^{M-1} Z_m$, then the modulus of Z, $R = |Z|$, has the following PDF*

$$f_R(r) = \frac{4r^M}{\Gamma(M)\cdot\left(\sigma_{Y_1}\sigma_{Y_2}\right)^{M+1}}\mathbb{K}_{M-1}\left(\frac{2r}{\sigma_{Y_1}\sigma_{Y_2}}\right), \tag{9}$$

where $\mathbb{K}_M(\cdot)$ is the M-th order modified Bessel function of the second kind.

Proof: See Appendix B.

In our study, we consider that each TD channel realization has a power normalized to one, which also induces that the variances of RVs H_n^k and $\overline{H}_n^k$ are equal to one. Substituting the result of the theorem into (4), we obtain the following closed-form NMSE expression at the unintended position

$$NMSE \approx \frac{4\gamma^{-1}}{\Gamma(M)} \int_0^{\infty} \frac{z^M}{z^2/U^2 + \gamma^{-1}} \mathbb{K}_{M-1}(2z)\, dz. \tag{10}$$

In order to get a tractable NMSE expression to further evaluate the asymptotic behaviors, we apply the series expansion of the modified Bessel function of the second kind [21, eq. (24)]

$$\mathbb{K}_M(x) \approx \sum_{q=0}^{D} \sum_{l=q}^{D} \Psi(M,l,q) \cdot \mathrm{e}^{-x} \cdot x^{q-M}, \tag{11}$$

where D specifies the number of expansion terms, $\Psi(M,l,q)$ is a coefficient given by

$$\Psi(M,l,q) = \frac{(-1)^q \sqrt{\pi} \cdot \Gamma(2M) \cdot \Gamma\left(\frac{1}{2} + l - M\right) \cdot \mathbb{L}(l,q)}{2^{M-q} \cdot \Gamma\left(\frac{1}{2} - M\right) \cdot \Gamma\left(\frac{1}{2} + l + M\right) \cdot l!} \tag{12}$$

and $\mathbb{L}(l,q) = \begin{pmatrix} l-1 \\ q-1 \end{pmatrix} \frac{l!}{q!}$ for $\forall l, q > 0$ is the Lah number [21] with the conventions $\mathbb{L}(0,0) = 1$, $\mathbb{L}(l,0) = 0$, $\mathbb{L}(l,1) = l!$ for $\forall l > 0$.

Since the order $M-1$ of the modified Bessel function of the second kind in (10) is a non-negative integer number, the series representation (11) converges except for $M - 1 = 0$ [21]. However, $\mathbb{K}_0(x)$ can be computed from the series representations of $\mathbb{K}_1(x)$ and $\mathbb{K}_2(x)$ based on the recurrence identity: $\mathbb{K}_0(x) = \mathbb{K}_2(x) - 2x^{-1}\mathbb{K}_1(x)$ [22].

Based on the derivation in the Appendix C, the tractable closed-form NMSE approximation, $f_{unint}(\gamma, U, N_T)$, can be obtained

$$f_{unint}(\gamma,U,N_T) \approx \begin{cases} \dfrac{1}{(UN_T-1)!} \displaystyle\sum_{q=0}^{D} \mathbb{G}_{UN_T}(q) \Bigg[\dfrac{1}{2^{UN_T-1}} \Gamma_{low}\left(q+2, 2U\gamma^{-1/2}\right) \\ \qquad - \dfrac{1}{2^{UN_T+1}U^2\gamma^{-1}} \Gamma_{low}\left(q+4, 2U\gamma^{-1/2}\right) + \dfrac{1}{2^{UN_T+3}U^4\gamma^{-2}} \Gamma_{low}\left(q+6, 2U\gamma^{-1/2}\right) \\ \qquad + \dfrac{U^2\gamma^{-1}}{2^{UN_T-3}} \Gamma_{up}\left(q, 2U\gamma^{-1/2}\right) - \dfrac{U^4\gamma^{-2}}{2^{UN_T-5}} \Gamma_{up}\left(q-2, 2U\gamma^{-1/2}\right) \Bigg], & \text{if} \quad UN_T > 1 \\ \displaystyle\sum_{q=0}^{D} \mathbb{G}_1(q) \Big[\Gamma_{low}\left(q, 2U\gamma^{-1/2}\right) - \dfrac{1}{4 \cdot U^2\gamma^{-1}} \Gamma_{low}\left(q+2, 2U\gamma^{-1/2}\right) \\ \qquad + \dfrac{1}{16 \cdot U^4\gamma^{-2}} \Gamma_{low}\left(q+4, 2U\gamma^{-1/2}\right) + 4 \cdot U^2\gamma^{-1} \Gamma_{up}\left(q-2, 2U\gamma^{-1/2}\right) \\ \qquad - 16 \cdot U^4\gamma^{-2} \Gamma_{up}\left(q-4, 2U\gamma^{-1/2}\right) \Big], & \text{if} \quad UN_T = 1 \end{cases} \tag{13}$$

in which $\mathbb{G}_{UN_T}(q)$ is calculated as follows

$$\begin{cases} \mathbb{G}_{UN_T}(q) = \sum_{l=q}^{D} \Psi\left(UN_T - 1, l, q\right), & \text{if } UN_T > 1 \\ \mathbb{G}_1(q) = \sum_{l=q}^{D} \left(\Psi(2, l, q) - 2 \cdot \Psi(1, l, q)\right), & \text{if } UN_T = 1 \end{cases} \tag{14}$$

The FG at a certain NMSE can finally be deduced by

$$\begin{aligned} FG &= \gamma_{unint} - \gamma_{int} \\ \text{s.t.} \quad & f_{int}(\gamma_{int}, U, N_T) = f_{unint}(\gamma_{unint}, U, N_T) \end{aligned} \tag{15}$$

5. Asymptotic Analysis

We derive here the asymptotic (in SNRs, BOFs U and the number of antennas N_T parameters) behaviors of the NMSE approximations to gain insights.

- *At the intended position:*

Considering (6) at high SNR, we have $U\gamma^{-1/2} \approx 0$, and therefore $\Gamma_{low}\left(s, U\gamma^{-1/2}\right) \approx 0$ and $\Gamma_{up}\left(s, U\gamma^{-1/2}\right) \approx \Gamma(s)$. In (6) the value of the fourth term is much bigger than that of the fifth term. The NMSE at high SNR, $f_{int}^{high}\left(\gamma, U, N_T\right)$, can be approximated by

$$f_{int}^{high}\left(\gamma, U, N_T\right) \approx \frac{U^2\gamma^{-1}\Gamma\left(UN_T - 2\right)}{\left(UN_T - 1\right)!}, \tag{16}$$

In the case a is a positive integer, $\Gamma(a) = (a-1)!$. Considering $UN_T > 2$, (16) is further simplified as follows

$$f_{int}^{high}\left(\gamma, U, N_T\right) \approx \frac{\gamma^{-1}}{\left(N_T - 1/U\right)\left(N_T - 2/U\right)} \overset{U\to+\infty}{\to} \frac{\gamma^{-1}}{\left(N_T\right)^2}. \tag{17}$$

It reveals that when the BOF is sufficiently high, the NMSE can only be reduced by increasing the number of antennas, as shown later in the simulations.

Considering (6) at low SNR, the proposed NMSE approximation $f_{int}^{low}\left(\gamma, U, N_T\right)$ is

$$f_{int}^{low}\left(\gamma, U, N_T\right) \approx \frac{\Gamma_{low}\left(UN_T, U\gamma^{-1/2}\right)}{\left(UN_T - 1\right)!} \tag{18}$$

because in (6) the second and third terms are smaller than the first term, whereas the fourth and fifth terms are approximately equal to 0. Using the series expansion $\Gamma_{low}(a, t) = t^a\Gamma(a)\,\mathrm{e}^{-t}\sum_{k=0}^{\infty} t^k \big/ \Gamma(a + k + 1)$ [23, eqs. (8.2.6) and (8.7.1)] and after some manipulations, we can obtain the following approximation

$$f_{int}^{low}\left(\gamma, U, N_T\right) \approx 1 - \mathrm{e}^{-U\gamma^{-1/2}} \sum_{k=1}^{UN_T} \frac{\left(U\gamma^{-1/2}\right)^{UN_T - k}}{\left(UN_T - k\right)!}. \tag{19}$$

It can be seen that the same conclusion as for $f_{int}^{high}\left(\gamma, U, N_T\right)$ can be drawn from (19). If the BOF U is sufficiently high, the $f_{int}^{low}\left(\gamma, U, N_T\right)$ can only be reduced by increasing the number of antennas N_T. Because for a fixed value of N_T, the term $\mathrm{e}^{-U\gamma^{-1/2}}$ reduces faster than the summation term of (19) when increasing U, resulting in an un-changed

$f_{int}^{low}\left(\gamma, U, N_T\right)$ value if U is sufficiently high. In the case U is set to a certain value, $f_{int}^{low}\left(\gamma, U, N_T\right)$ value can still be reduced further when increasing N_T as more terms are added in the summation.

- At the unintended position:

At high SNR, similar to the analysis at the intended position, only the terms with $\Gamma_{up}(\cdot)$ have a significant contribution to the NMSE. Considering $UN_T > 1$ for the sake of simplicity, (13) can be approximated to

$$f_{unint}^{high}\left(\gamma, U, N_T\right) \approx \frac{\gamma^{-1}\sqrt{\pi}U^2 \cdot \Gamma\left(2\left(UN_T-1\right)\right)}{2^{2UN_T-4}\cdot\Gamma\left(UN_T\right)} \sum_{q=0}^{D}\sum_{l=q}^{D} \frac{(-2)^q \Gamma\left(\frac{3}{2}-UN_T+l\right)\mathbb{L}\left(l,q\right)\Gamma_{up}\left(q, 2U\gamma^{-1/2}\right)}{\Gamma\left(\frac{3}{2}-UN_T\right)\Gamma\left(UN_T-\frac{1}{2}+q\right)q!} \tag{20}$$

By virtue of $\Gamma\left(UN_T\right) = \left(UN_T-1\right)\Gamma\left(UN_T-1\right)$ and applying the Legendre duplication formula to $\Gamma\left(2\left(UN_T-1\right)\right)$, (20) is rewritten as

$$f_{unint}^{high}\left(\gamma, U, N_T\right) \approx 2\gamma^{-1}\frac{U^2}{\left(UN_T-1\right)} \sum_{q=1}^{D}\sum_{l=q}^{D} \frac{(-2)^q \mathbb{L}\left(l,q\right)\Gamma\left(q\right)\Gamma\left(UN_T-\frac{1}{2}\right)\Gamma\left(\frac{3}{2}-UN_T+l\right)}{q!\Gamma\left(\frac{3}{2}-UN_T\right)\Gamma\left(UN_T-\frac{1}{2}+q\right)} \tag{21}$$

It can be observed that both numerator and denominator of the fraction term inside the summation of (21) are propotional to $U^2N_T^2$, therefore this fraction asymptotically converges to a constant when increasing UN_T. Considering U and N_T as the variables, $f_{unint}^{high}\left(\gamma, U, N_T\right)$ is propotional to the following expression

$$f_{unint}^{high}\left(\gamma, U, N_T\right) \propto \frac{U^2}{UN_T-1} \tag{22}$$

It can be concluded from (22) that increasing the BOF U causes the increase of NMSE (or equivalently decreases the focusing gain). The NMSE can be reduced by using more transmit antennas.

The same analysis and conclusion can be drawn for low SNRs, we skip it as it does not bring any additional insight.

Table 1
PDP of the Extended Pedestrian A (EPA) channel.

Excess tap delay (ns)	Relative power (dB)
0	0.0
30	-1.0
70	-2.0
90	-3.0
110	-8.0
190	-17.2
410	-20.8

6. Simulation Results

We consider a 256-subcarrier MISO OFDM system, i.e., $Q = 256$. A multi-path channel of type Extended Pedestrian A (EPA) [24] is used in the simulations. Its power delay profile (PDP) is given in Table 1. The overall channel power is normalized to unity for each channel realization. We assume that the channel is perfectly known at the transmitter. The impact of imperfect channel estimation on the TR-based system performance has been studied in [25] (and references therein), but is beyond the scope of this paper. Note that, we set the number of the expansion term of modified Bessel function $D = 20$ in the following computations. The analytical results at the intended and unintended positions are presented by the solid-lines and dashed-lines, respectively. The numerical results with respect to either intended or unintended positions are plotted with marker symbols.

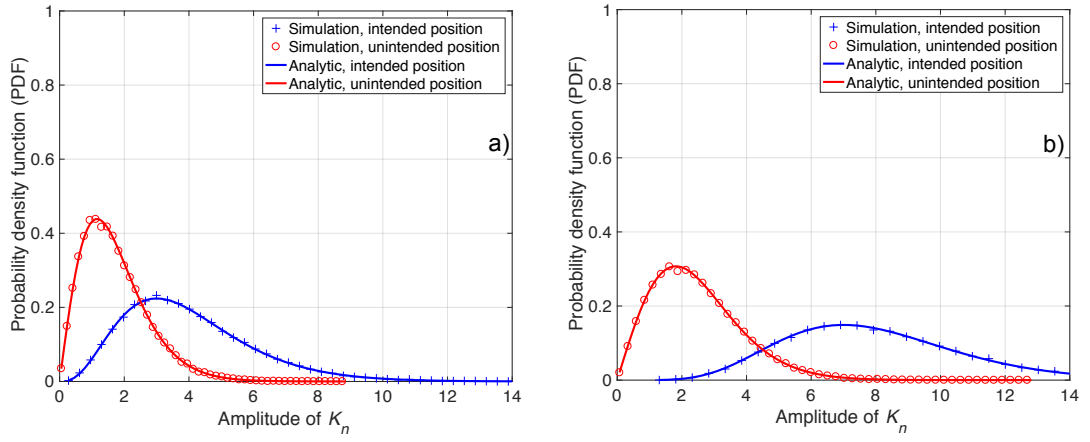

Figure 2: Probability density function (PDF) envelopes of the RV K_n at the intended and unintended positions. a) $M = 4$; b) $M = 8$.

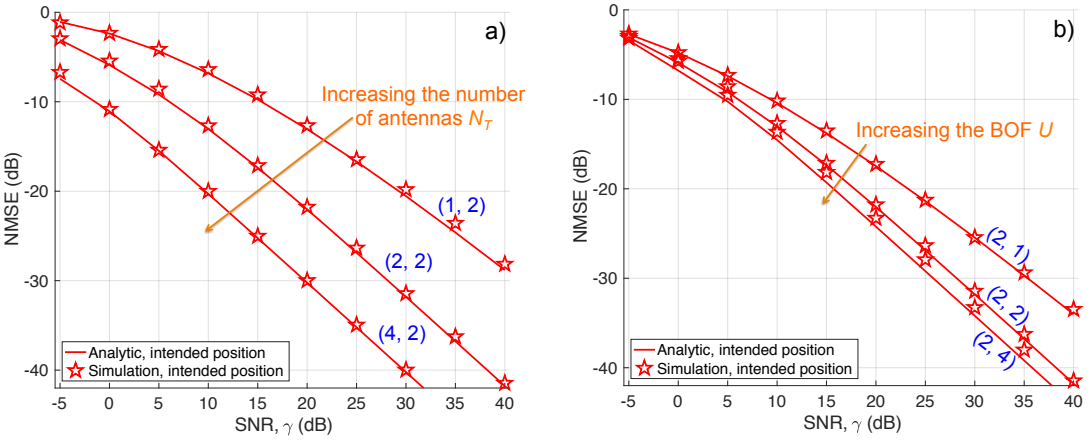

Figure 3: NMSE versus SNR at the intended position. a) Different number of antennas when $U = 2$, b) Different BOFs when $N_T = 2$. The couple (N_T, U) is indicated on each curve.

As the RV K_n in (4) can intuitively be related to the diversity gain given by the TR focusing and the use of multiple antennas, we consider the distribution of K_n at the intended and unintended positions in Fig. 2 when $M = 4$ and $M = 8$ based on derived PDFs. It can be seen that the analytical PDFs match the numerical ones[2]. At the intended position, the TR precoding matches the channel, while there is a mismatch between the precoding and channel at the unintended position. Consequently, the values of RV K_n at the intended position are distributed in a wider range than that at the unintended position (i.e., when $M = 4$, the value of K_n is mainly distributed from 0.2 up to 11 at the intended position, while it falls between 0.1 and 5 at the unintended position). When increasing M from 4 to 8, the distribution of K_n value increases accordingly. The bigger value of K_n can get, the more diversity gain can achieve. In other words, the bigger value of K_n in (4) leads to a smaller NMSE value. It implicitly explains that the NMSE at the intended position is smaller than that at the unintended position when increasing M.

In the first step, we evaluate the NMSE as a function of the SNR at the intended position in Fig. 3. Fig. 3(a) shows NMSE evolution for different number of antennas, when U is equal to 2. Fig. 3(b) presents NMSE evolution for different BOFs, when N_T is set to 2. As expected, the analytical closed-form NMSEs match the ones obtained by simulations, confirming the correctness of our derivation in (6). The simulation results also confirm our previous observation that when increasing the BOF, the NMSE (and hence the spatio-temporal focusing) converges asymptotically

[2]Due to the normalized channel generation, the variance of K_n is equal to one. Other values of variances of K_n are also verified but not shown here.

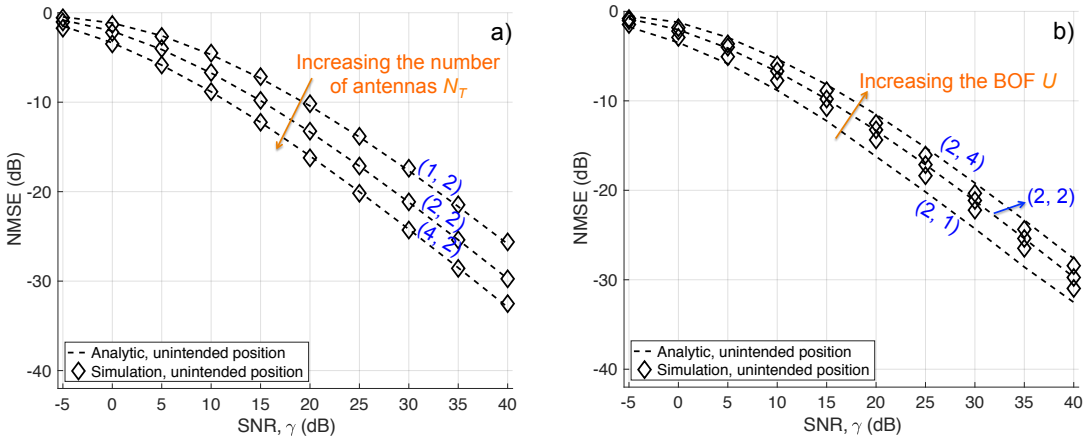

Figure 4: NMSE versus SNR at the unintended position. a) Different number of antennas when $BOF = 2$, b) Different BOFs when $N_T = 2$. The couple (N_T, U) is indicated on each curve.

to an NMSE lower bound. It is observed that increasing the number of antennas continuously provides the focusing gain. For instance, in order to obtain a NMSE $= -20$ dB, by changing the number of antennas from one to two, we achieve a SNR gain of about 12 dB, while by using a BOF of two instead of one, we can only obtain a SNR gain of about 6 dB.

We now evaluate the NMSE as a function of the SNR at the unintended position in Fig. 4 with different number of antennas when U is equal to 2 (Fig. 4(a)) and with different BOFs when N_T is set to 2 (Fig. 4(b)). Similar to the results at the intended position, the numerical NMSEs follow the predicted analytical ones in (13). The simulation results also confirm the asymptotic analyses that the NMSE can only improve by increasing the number of antennas, while, in contrast to the case at the intended position, increasing the BOF gives a poorer MSE. For instance, at NMSE equal to -20 dB, by changing the number of antennas from one to two, we achieve about 4 dB SNR gain (much less than that at the intended position), while by using a BOF of two instead of one, the SNR loss is about 0.6 dB.

The MSEs at the intended and unintended positions are compared in Fig. 5. It can be observed that when changing from the no-focusing-gain case ($U = N_T = 1$) to the case where $U = N_T = 4$ and considering the NMSE $= -20$ dB, the SNR gain at the intended position is about 22 dB bigger than that at the unintended position, confirming again the focusing effect provided by the TR precoding. It is also reminded that the SNR gain at the unintended position is provided by only the increase of the number of antennas. Surprisingly, we observe from the no-focusing-gain case that the NMSE value at the unintended position is smaller than that at the intended position for the moderate and high SNRs (Fig. 5). Rigorously, we can explain this fact based on the equations (6) and (13) by considering their monotonicities in the interesting SNR range. Intuitively, it can be explained because the precoded channels at the unintended position are complex, while the precoded channels at the intended position are real, resulting in a less deep fading probability at the subcarrier-level of the equivalent channel magnitude.

Finally, we investigate the focusing gain when varying the number of antennas and BOFs and the targeted NMSE is fixed to -10 dB. The results are presented in Fig. 6. The numerical results confirm again the observation made in the analyses that by increasing either the number of antennas or BOFs, we can improve the focusing gain. It is worth reminding that the focusing gain is defined by the SNR gain necessary to keep the MSE at a fixed value. At the intended position, the RV K_n is built constructively thanks to the TR precoding of the signal with the corresponding CFR. This leads to the reduction of the NMSE and hence improves the focusing gain, especially when increasing BOFs (associated with the frequency diversity gain). On the contrary, at the unintended position, the RV K_n is constructed destructively from $(H_n^k)^*$ and $\overline{H}_n^k$ associated with the CFR component at the unintended position, because of their spatial independence. This causes the increase in the NMSE in (3) when increasing the BOFs. In the case we increase the number of antennas, the NMSEs in both intended and unintended positions are reduced thanks to the spatial diversity gain. However, the SNR gain at the unintended position is smaller than that at the intended position, since the spatial diversity gain at the unintended position can partially compensates for the destructive construction of the RV K_n (originating from the BOF). It should also be noted that when the BOF value is high, the assumption of the

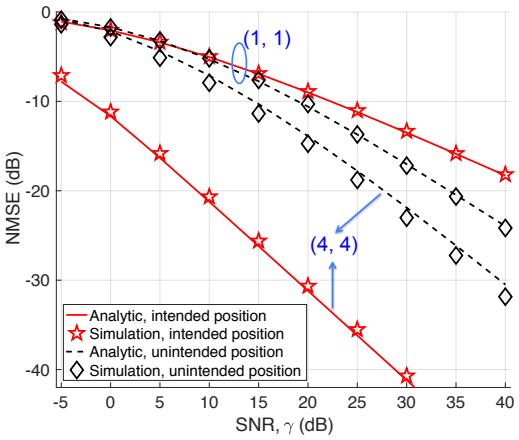

Figure 5: NMSE versus SNR at both intended and unintended positions when increasing the number of antennas and BOFs. The couple (N_T, U) is indicated on each curve.

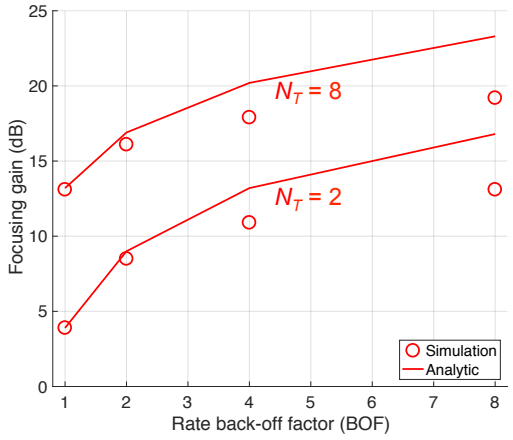

Figure 6: Focusing gain at the targeted NMSE of -10 dB as a function of the rate back-off factor when the number of antennas are equal to 2 and 8.

statistical independence among RVs H_n does not hold so that there are some mismatches between the analytical and numerical results.

7. Conclusion

We have investigated the FD/TR precoding in the MISO OFDM communication system with BOFs different to one, when communicating to either intended or unintended positions. We have also verified the focusing gain (provided by the FD/TR precoding), which is defined as the SNR gain required to maintain a fixed value of MSE. By evaluating the NMSE, we have shown that, at the intended position, increasing either the BOF or the number of antennas improves the focusing gain. Conversely, at the unintended position, the useful received power is lower. The approximated NMSE expressions at the intended and unintended positions and the subsequent focusing gain have been derived and validated through simulations.

References

[1] Y. Chen, Y.-H. Yang, F. Han, and K. J. R. Liu, "Time-reversal wideband communications," IEEE Signal Process. Lett., vol. 20, no. 12, pp. 1219–1222, Dec. 2013.

[2] M. Emami, M. Vu, J. Hansen, A. J. Paulraj, and G. Papanicolaou, "Matched filtering with rate back-off for low complexity communications in very large delay spread channels," Proc. Conf. Record 38th Asilomar Conf. Signals Syst. Comput., vol. 1, pp. 218–222, 2004.

[3] T. Dubois, M. Helard, M. Crussiere and C. Germond, "Performance of time reversal precoding technique for MISO-OFDM systems," EURASIP J. Wirel. Commun. Netw., article # 2013:260, 2013.
[4] T.-H. Nguyen, M. Van Eeckhaute, J.-F. Determe, J. Louveaux, P. De Doncker and F. Horlin, "Analysis of residual CFO impact on downlink massive MISO systems," IET Electron. Lett., vol. 55, no. 18, pp. 1017–1019, Sep. 2019.
[5] T.-H. Nguyen, S. Monfared, J.-F. Determe, J. Louveaux, P. De Doncker and F. Horlin, "Performance analysis of frequency domain precoding time-reversal MISO OFDM systems," IEEE Commun. Lett., Early Access, Nov. 2019.
[6] M. Fink, "Acoustic time-reversal mirrors," Imaging of Complex Media with Acoustic and Seismic Waves (M. Fink, W. Kuperman, J.-P. Montagner, and A. Tourin, eds.), Topics in Applied Physics, Springer Berlin Heidelberg, vol. 84, 2002.
[7] B. Bogert, "Demonstration of delay distortion correction by time-reversal techniques," IRE Trans. Commun. Syst., vol. 5, no. 3, pp. 2–7, Dec. 1957.
[8] F. Amoroso, "Optimum realizable transmitter waveforms for high-speed data transmission," IEEE Trans. Commun. Technol., vol. 14, no. 1, pp. 8–13, Feb. 1966.
[9] M. Fink, C. Prada, F. Wu and D. Cassereau, "Self focusing in inhomogeneous media with time reversal acoustic mirrors," Proceedings of Ultrasonics Symposium, vol. 2, pp. 681–686, Oct. 1989.
[10] A. J. Devaney, "Time reversal imaging of obscured targets from multi-static data," IEEE Trans. Antennas Propag., vol. 53, no. 5, pp. 1600–1610, May 2005.
[11] Y. Jin, J. M. F. Moura, "Time-reversal detection using antenna arrays," IEEE Trans. Signal Process., vol. 57, no. 4, pp. 1396–1414, Apr. 2009.
[12] Y. Chen, B. Wang, Y. Han, H. Q. Lai, Z. Safar, and K. J. R. Liu, "Why Time Reversal for Future 5G Wireless? [Perspectives]," IEEE Signal Process. Mag., vol. 33, no. 2, pp. 17–26, Mar. 2016.
[13] Q. Xu, P. Ren, Q. Du, and L. Sun, "Security-aware waveform and artificial noise design for time-reversal-based transmission," IEEE Trans. Veh. Technol., vol. 67, no. 6, pp. 5486–5490, Jun. 2018.
[14] Z.-H. Wu, Y. Han, Y. Chen, and K. J. R. Liu, "A time-reversal paradigm for indoor positioning system," IEEE Trans. Veh. Technol., vol. 64, no. 4, pp. 1331–1339, Apr. 2015.
[15] T.-H. Nguyen, J. Louveaux, P. De Doncker, and F. Horlin, "Impact of I/Q imbalance on time reversal-based indoor positioning systems," IEEE 14th International Conference on Wireless and Mobile Computing, Networking and Communications (WiMob), pp. 36–41, Oct. 2018.
[16] T.-H. Nguyen, S. Golstein, J. Louveaux, P. De Doncker, and F. Horlin, "Performance analysis and mitigation method for I/Q imbalance-impaired time reversal-based indoor positioning systems," IEEE 90th Vehicular Technology Conference (VTC2019-Fall), Sep. 2019.
[17] Q. Xu, Y. Chen, B. Wang and K. J. R. Liu, "TRIEDS: Wireless events detection through the wall," IEEE Internet Things J., vol. 4, no. 3, pp. 723–735, Jun. 2017.
[18] C. Chen, Y. Han, Y. Chen, H. Q. Lai, F. Zhang, B. Wang, and K. J. R. Liu, "TR-BREATH: Time-reversal breathing rate estimation and detection," IEEE Trans. Biomed. Eng., vol. 65, no. 3, pp. 489–501, Mar. 2018.
[19] M. Speth, S. Fechtel, G. Fock, and H. Meyr, "Optimum receiver design for wireless broad-band systems using OFDM - Part I," IEEE Trans. Commun., vol. 47, no. 11, pp. 1668–1677, Nov. 1999.
[20] A. Papoulis, "Probability, random variables and stochastic processes," McGraw-Hill Companies, 3rd edition, 1991.
[21] M. M. Molu, P. Xiao, M. Khalily, L. Zhang, and R. Tafazolli, "A novel equivalent definition of modified Bessel functions for performance analysis of multi-hop wireless communication systems," IEEE Access, vol. 5, pp. 7594–7605, May 2017.
[22] http://functions.wolfram.com/Bessel-TypeFunctions/BesselK. *Access on Jan. 10th 2019.*
[23] NIST Digital Library of Mathematical Functions, link: https://dlmf.nist.gov/8.
[24] 3GPP - TS 36.101, "User Equipment (UE) Radio Transmission and Reception." 3rd Generation Partnership Project; Technical Specification Group Radio Access Network; Evolved Universal Terrestrial Radio Access (E-UTRA). URL: http://www.3gpp.org.
[25] S. Alizadeh, H. K. Bizaki, and M. Okhovvat, "Effect of channel estimation error on performance of time reversal-UWB communication system and its compensation by pre-filter," IET Commun., vol. 6, no. 12, pp. 1781–1794, Aug. 2012.
[26] N. O'Donoughue, and J. M. F. Moura, "On the product of independent complex Gaussians," IEEE Trans. Signal Process., vol. 60, no. 3, pp. 1050–1063, Mar. 2012.
[27] I. S. Gradshteyn, and I. M. Ryzhik, "Tables of integrals, series and products," San Diego Academic, 7th edition, 2007.

A. Appendix I

At the intended position, based on the PDF of K_n, (5) can be rewritten as

$$\begin{aligned} NMSE &\approx \int_0^{\infty} \frac{\gamma^{-1}}{z^2/U^2+\gamma^{-1}} \frac{z^{M-1}}{(M-1)!} \mathrm{e}^{-z} dz \\ &\approx \frac{1}{(M-1)!} \left(\int_0^{U\gamma^{-1/2}} \frac{\gamma^{-1}}{z^2/U^2+\gamma^{-1}} z^{M-1} \mathrm{e}^{-z} dz + \int_{U\gamma^{-1/2}}^{\infty} \frac{\gamma^{-1}}{z^2/U^2+\gamma^{-1}} z^{M-1} \mathrm{e}^{-z} dz \right). \end{aligned} \tag{23}$$

Splitting the NMSE formula into two parts $T_1 = \int_0^{U\gamma^{-1/2}} \frac{\gamma^{-1} z^{M-1} \mathrm{e}^{-z}}{z^2/U^2+\gamma^{-1}} dz$ and $T_2 = \int_{U\gamma^{-1/2}}^{\infty} \frac{\gamma^{-1} z^{M-1} \mathrm{e}^{-z}}{z^2/U^2+\gamma^{-1}} dz$ ensures that

the integrals can be simplified in the two ranges of interest. More particularly, T_1 can be rewritten as

$$T_1 = \int_0^{U\gamma^{-1/2}} \left(1 + \frac{z^2}{U^2\gamma^{-1}}\right)^{-1} z^{M-1}\mathrm{e}^{-z}dz \approx \int_0^{U\gamma^{-1/2}} \left(1 - \frac{z^2}{U^2\gamma^{-1}} + \frac{z^4}{U^4\gamma^{-2}}\right) z^{M-1}\mathrm{e}^{-z}dz, \tag{24}$$

where the approximation is achieved by using the Taylor expansion $(1+x)^{-1} = \sum_{n=0}^{\infty}(-x)^n$ that converges on the range of the integral $\left(0, U\gamma^{-1/2}\right)$, as $z^2/\left(U^2\gamma^{-1}\right) < 1$. Substituting the lower incomplete Gamma function defined in (7) into (24), we obtain the closed-form expression of T_1

$$T_1 \approx \Gamma_{low}\left(M, U\gamma^{-1/2}\right) - \frac{1}{U^2\gamma^{-1}}\Gamma_{low}\left(M+2, U\gamma^{-1/2}\right) + \frac{1}{U^4\gamma^{-2}}\Gamma_{low}\left(M+4, U\gamma^{-1/2}\right). \tag{25}$$

Due to the fact that $U^2\gamma^{-1}/z^2 < 1$, we can apply again the Taylor expansion to T_2 that ensures the convergence on the range of the integral $\left(U\gamma^{-1/2}, \infty\right)$, T_2 can be rewritten as follows

$$T_2 = \int_{U\gamma^{-1/2}}^{\infty} U^2\gamma^{-1}z^{-2}\left(1 + \frac{U^2\gamma^{-1}}{z^2}\right)^{-1} z^{M-1}\mathrm{e}^{-z}dz \approx \int_{U\gamma^{-1/2}}^{\infty} U^2\gamma^{-1}z^{-2}\left(1 - \frac{U^2\gamma^{-1}}{z^2}\right) z^{M-1}\mathrm{e}^{-z}dz. \tag{26}$$

Using the definition of the upper incomplete Gamma function (8), the closed-form expression of T_2 can be derived

$$T_2 \approx U^2\gamma^{-1}\Gamma_{up}\left(M-2, U\gamma^{-1/2}\right) - U^4\gamma^{-2}\Gamma_{up}\left(M-4, U\gamma^{-1/2}\right). \tag{27}$$

Finally, substituting (25) and (27) into (23) and using the fact that $M = UN_T$, we achieve the closed-form NMSE expression at the intended position as in (6).

B. Appendix II

Considering a RV $Z_m = Y_{1,m} \cdot Y_{2,m}$, where $Y_{1,m} \sim \mathcal{CN}(0, \sigma^2_{Y_1})$, $Y_{2,m} \sim \mathcal{CN}(0, \sigma^2_{Y_2})$, and defining $R_m = |Z_m|$, $\Theta_m = \angle Z_m$, where $\angle$ is the angle operator, the marginal joint PDF of R_m and Θ_m has been derived in [26, eq. (17)] as follows

$$f_{R_m,\Theta_m}\left(r_m, \theta_m\right) = \frac{2r_m}{\pi\sigma^2_{Y_1}\sigma^2_{Y_2}}\mathbb{K}_0\left(\frac{2r_m}{\sigma_{Y_1}\sigma_{Y_2}}\right). \tag{28}$$

where $\mathbb{K}_M(\cdot)$ is the M-th order modified Bessel function of the second kind. The characteristic function (CF) of R_m and Θ_m can be written as

$$\begin{aligned}\psi_{R_m,\Theta_m}\left(j\omega_1, j\omega_2\right) &= \int_{-\infty}^{\infty}\int_{-\infty}^{\infty} \mathrm{e}^{\left(j\omega_1 r_m\cos\theta_m + j\omega_2 r_m \sin\theta_m\right)} \cdot f_{R_m,\Theta_m}\left(r_m, \theta_m\right) dr_m d\theta_m \\ &= \int_0^{\infty}\int_0^{2\pi} \mathrm{e}^{\left(j\omega_1 r_m\cos\theta_m + j\omega_2 r_m \sin\theta_m\right)} d\theta_m \cdot \frac{2}{\pi\sigma^2_{Y_1}\sigma^2_{Y_2}} r_m \mathbb{K}_0\left(\frac{2r_m}{\sigma_{Y_1}\sigma_{Y_2}}\right) dr_m\end{aligned} \tag{29}$$

Applying the equation [27, eq. (3.937-2)] to the inner integral of (29), we can obtain the following result

$$\int_0^{2\pi} \mathrm{e}^{\left(j\omega_1 r_m\cos\theta_m + j\omega_2 r_m \sin\theta_m\right)} d\theta_m = 2\pi\mathbb{I}_0\left(jr_m\sqrt{\omega_1^2 + \omega_2^2}\right) \tag{30}$$

where $\mathbb{I}_M(\cdot)$ is the modified Bessel function of the first kind with order M. The CF of R_m and Θ_m can be rewritten as

$$\psi_{R_m,\Theta_m}\left(j\omega_1, j\omega_2\right) = \frac{4}{\sigma_{Y_1}^2\sigma_{Y_2}^2}\cdot\int_0^\infty r_m\cdot\mathbb{I}_0\left(jr_m\sqrt{\omega_1^2+\omega_2^2}\right)\cdot\mathbb{K}_0\left(\frac{2r_m}{\sigma_{Y_1}\sigma_{Y_2}}\right)dr_m \tag{31}$$

Using the integration formula [27, eq. (6.576-3)], we achieve the CF as follows

$$\psi_{R_m,\Theta_m}\left(j\omega_1, j\omega_2\right) = {}_2F_1\left(1,1;1;-\frac{\sigma_{Y_1}^2\sigma_{Y_2}^2\left(\omega_1^2+\omega_2^2\right)}{4}\right), \tag{32}$$

where ${}_2F_1\left(\alpha,\beta;\lambda;z\right)$ is the Gaussian hypergeometric function. Due to the fact that ${}_2F_1\left(\alpha,1;1;z\right) = (1-z)^{-\alpha}$, (32) becomes

$$\psi_{R_m,\Theta_m}\left(j\omega_1, j\omega_2\right) = \left(1+\frac{\sigma_{Y_1}^2\sigma_{Y_2}^2\left(\omega_1^2+\omega_2^2\right)}{4}\right)^{-1}. \tag{33}$$

Considering the RV $Z = \sum_{m=0}^{M-1} Z_m$ with its modulus $R = |Z|$ and its argument $\Theta = \angle Z$ and assuming that Z_m and Z_n are statistically independent for $\forall m \neq n$, the CF of R_m and Θ_m corresponding to the RV Z can be derived based on the properties of CF as follows

$$\psi_{R,\Theta}\left(j\omega_1, j\omega_2\right) = \left(1+\frac{\sigma_{Y_1}^2\sigma_{Y_2}^2\left(\omega_1^2+\omega_2^2\right)}{4}\right)^{-M}. \tag{34}$$

Inverting the CF $\psi_{R,\Theta}\left(j\omega_1, j\omega_2\right)$, we can obtain the PDF of Z. Instead of directly inverting this CF, which is a non-trivial problem, we consider the following joint PDF

$$f_{R,\Theta}\left(r,\theta\right) = \frac{2r^M}{\pi\cdot\Gamma\left(M\right)\cdot\left(\sigma_{Y_1}\sigma_{Y_2}\right)^{M+1}}\mathbb{K}_{M-1}\left(\frac{2r}{\sigma_{Y_1}\sigma_{Y_2}}\right). \tag{35}$$

After carrying out the same manipulations as for $f_{R_m,\Theta_m}\left(r_m,\theta_m\right)$ (from (29) to (33)), we get the same CF as in (34). Therefore, we can conclude that $f_{R,\Theta}\left(r,\theta\right)$ function in (35) is the marginal joint PDF of the RV Z. Integrating the joint PDF over the RV θ, we obtain the PDF of $|Z|$ as in (9).

C. Appendix III

From (11) and (14), $\mathbb{K}_{M-1}(2z)$ in (10) can be approximated by

$$\mathbb{K}_{M-1}\left(2z\right) \approx \begin{cases} e^{-2z}\sum\limits_{q=0}^{D}\mathbb{G}_M\left(q\right)\cdot\left(2z\right)^{q-M+1}, & \text{if } M>1 \\ e^{-2z}\sum\limits_{q=0}^{D}\mathbb{G}_1\left(q\right)\cdot\left(2z\right)^{q-2}, & \text{if } M=1 \end{cases} \tag{36}$$

Similar to the derivation in the Appendix A, we split the NMSE at the unintended position (10) into two integrals to ensure the convergence when applying the Taylor expansion. More particularly, (10) can be rewritten as

$$NMSE \approx \frac{4}{\Gamma(M)} \int_0^{U\gamma^{-1/2}} \left(1+\frac{z^2}{U^2\gamma^{-1}}\right)^{-1} z^M \mathbb{K}_{M-1}(2z)\,dz + \frac{4}{\Gamma(M)} \int_{U\gamma^{-1/2}}^{\infty} U^2\gamma^{-1}\left(1+\frac{U^2\gamma^{-1}}{z^2}\right)^{-1} z^{M-2}\mathbb{K}_{M-1}(2z)\,dz. \tag{37}$$

Applying the Taylor series expansion to (37), we obtain the following NMSE approximation

$$\begin{aligned} NMSE \approx{}& \frac{4}{\Gamma(M)} \int_0^{U\gamma^{-1/2}} z^M \mathbb{K}_{M-1}(2z)\,dz - \frac{4}{\Gamma(M)U^2\gamma^{-1}} \int_0^{U\gamma^{-1/2}} z^{M+2}\mathbb{K}_{M-1}(2z)\,dz \\ &+ \frac{4}{\Gamma(M)U^4\gamma^{-2}} \int_0^{U\gamma^{-1/2}} z^{M+4}\mathbb{K}_{M-1}(2z)\,dz + \frac{4U^2\gamma^{-1}}{\Gamma(M)} \int_{U\gamma^{-1/2}}^{\infty} z^{M-2}\mathbb{K}_{M-1}(2z)\,dz \\ &- \frac{4U^4\gamma^{-2}}{\Gamma(M)} \int_{U\gamma^{-1/2}}^{\infty} z^{M-4}\mathbb{K}_{M-1}(2z)\,dz. \end{aligned} \tag{38}$$

We derive the first integral in (38) using the approximation in (36) as follows

$$\begin{aligned} J_1 &= \frac{4}{\Gamma(M)} \int_0^{U\gamma^{-1/2}} z^M \mathbb{K}_{M-1}(2z)\,dz \\ &\approx \frac{4}{\Gamma(M)2^M} \begin{cases} \int_0^{U\gamma^{-1/2}} \sum_{q=0}^{D} \mathbb{G}_M(q)\cdot(2z)^{q+1}\cdot \mathrm{e}^{-2z} dz, & \text{if } M>1 \\ \int_0^{U\gamma^{-1/2}} \sum_{q=0}^{D} \mathbb{G}_1(q)\cdot(2z)^{q-1}\cdot \mathrm{e}^{-2z} dz, & \text{if } M=1 \end{cases} \end{aligned} \tag{39}$$

By changing the variable, i.e., $x = 2z$, after some manipulations, J_1 can be derived as follows

$$J_1 \approx \begin{cases} \frac{1}{(M-1)!2^{M-1}} \sum_{q=0}^{D} \mathbb{G}_M(q)\cdot\Gamma_{low}\left(q+2, 2U\gamma^{-1/2}\right), & \text{if } M>1 \\ \sum_{q=0}^{D} \mathbb{G}_1(q)\cdot\Gamma_{low}\left(q, 2U\gamma^{-1/2}\right), & \text{if } M=1 \end{cases} \tag{40}$$

Carrying out the same derivation for the four integrals left in (38), we obtain the following results

$$J_2 = \frac{4}{\Gamma(M)U^2\gamma^{-1}} \int_0^{U\gamma^{-1/2}} z^{M+2}\mathbb{K}_{M-1}(2z)\,dz$$

$$\approx \begin{cases} \dfrac{1}{U^2\gamma^{-1}\,(M-1)!2^{M+1}} \cdot \displaystyle\sum_{q=0}^{D} \mathbb{G}_M\,(q) \cdot \Gamma_{low}\left(q+4, 2U\gamma^{-1/2}\right), & \text{if } \ M>1 \\ \dfrac{1}{4U^2\gamma^{-1}} \displaystyle\sum_{q=0}^{D} \mathbb{G}_1\,(q) \cdot \Gamma_{low}\left(q+2, 2U\gamma^{-1/2}\right), & \text{if } \ M=1 \end{cases} \tag{41}$$

$$J_3 = \frac{4}{\Gamma(M)\,U^4\gamma^{-2}} \int_0^{U\gamma^{-1/2}} z^{M+4}\mathbb{K}_{M-1}(2z)\,dz$$

$$\approx \begin{cases} \dfrac{1}{U^4\gamma^{-2}\,(M-1)!2^{M+3}} \cdot \displaystyle\sum_{q=0}^{D} \mathbb{G}_M\,(q) \cdot \Gamma_{low}\left(q+6, 2U\gamma^{-1/2}\right), & \text{if } \ M>1 \\ \dfrac{1}{16U^4\gamma^{-2}} \displaystyle\sum_{q=0}^{D} \mathbb{G}_1\,(q) \cdot \Gamma_{low}\left(q+4, 2U\gamma^{-1/2}\right), & \text{if } \ M=1 \end{cases} \tag{42}$$

$$J_4 = \frac{4U^2\gamma^{-1}}{\Gamma(M)} \int_{U\gamma^{-1/2}}^{\infty} z^{M-2}\mathbb{K}_{M-1}(2z)\,dz$$

$$\approx \begin{cases} \dfrac{U^2\gamma^{-1}}{(M-1)!2^{M-3}} \displaystyle\sum_{q=0}^{D} \mathbb{G}_M\,(q) \cdot \Gamma_{up}\left(q, 2U\gamma^{-1/2}\right), & \text{if } \ M>1 \\ 4U^2\gamma^{-1} \displaystyle\sum_{q=0}^{D} \mathbb{G}_1\,(q) \cdot \Gamma_{up}\left(q-2, 2U\gamma^{-1/2}\right), & \text{if } \ M=1 \end{cases} \tag{43}$$

and

$$J_5 = \frac{4U^4\gamma^{-2}}{\Gamma(M)} \int_{U\gamma^{-1/2}}^{\infty} z^{M-4}\mathbb{K}_{M-1}(2z)\,dz$$

$$\approx \begin{cases} \dfrac{U^4\gamma^{-2}}{(M-1)!2^{M-5}} \displaystyle\sum_{q=0}^{D} \mathbb{G}_M\,(q) \cdot \Gamma_{up}\left(q-2, 2U\gamma^{-1/2}\right), & \text{if } \ M>1 \\ 16U^4\gamma^{-2} \displaystyle\sum_{q=0}^{D} \mathbb{G}_1\,(q) \cdot \Gamma_{up}\left(q-4, 2U\gamma^{-1/2}\right), & \text{if } \ M=1 \end{cases} \tag{44}$$

Due to the fact that $M = UN_T$, $\Gamma(M) = (M-1)!$ for a positive integer M, substituting (40), (41), (42), (43) and (44) into (38) yields the closed-form NMSE approximation as in (13).